ELSEVIER

NeuroImage

www.elsevier.com/locate/ynimg
NeuroImage 39 (2008) 1041–1050

Partial volume corrected image derived input functions for dynamic PET brain studies: Methodology and validation for [^{11}C]flumazenil

Jurgen E.M. Mourik,[a,*] Mark Lubberink,[a] Ursula M.H. Klumpers,[b] Emile F. Comans,[a] Adriaan A. Lammertsma,[a] and Ronald Boellaard[a]

[a]*Department of Nuclear Medicine and PET Research, VU University Medical Center, P.O. Box 7057, 1007 MB Amsterdam, The Netherlands*
[b]*Department of Psychiatry, VU University Medical Center, Amsterdam, The Netherlands*

Received 28 June 2007; revised 5 September 2007; accepted 13 October 2007

Extraction of arterial input functions from dynamic brain scans may obviate the need for arterial sampling and would increase the clinical applicability of quantitative PET studies. The aim of the present study was to evaluate applicability and accuracy of image derived input functions (IDIFs) following reconstruction based partial volume correction (PVC).

Settings for the PVC ordered subset expectation maximization (PVC-OSEM) reconstruction algorithm were varied. In addition, different methods for defining arterial regions of interest (ROI) in order to extract IDIFs were evaluated. [^{11}C]flumazenil data of 10 subjects were used in the present study. Results obtained with IDIFs were compared with those using standard on-line measured arterial input functions. These included areas under the curve (AUC) for peak (1–2 min) and tail (2–60 min), volume of distribution (V_T) obtained using Logan analysis, and V_T and K_1 obtained with a basis function implementation of a single tissue compartment model.

Best results were obtained with PVC-OSEM using 4 iterations and 16 subsets. Based on ^{11}C point source measurements, a 4.5 mm FWHM (full width at half maximum) resolution kernel was used to correct for partial volume effects. A ROI consisting of the four hottest pixels per plane (over the carotid arteries) was the best method to extract IDIFs. Excellent peak AUC ratios (0.99 ± 0.09) between IDIF and blood sampler input function (BSIF) were found. Furthermore, extracted IDIFs provided V_T and K_1 values that were very similar to those obtained using BSIFs.

The proposed method appears to be suitable for analysing [^{11}C] flumazenil data without the need for online arterial sampling.

Introduction

Positron emission tomography (PET) is a medical imaging technique that is used to study tissue function *in vivo* by imaging and measuring regional tracer concentrations of radiopharmaceuticals labelled with a positron emitter. A tracer model is needed to derive the tissue function under study from these measurements. Tracer kinetic modelling also requires measurement of the tracer time course in plasma, unless a reference tissue (Lammertsma et al., 1996; Lammertsma and Hume, 1996) can be found in which non-specific tracer uptake is identical to that in the tissue of interest. In general, arterial sampling is considered to be the gold standard for obtaining the arterial input function. However, arterial sampling is invasive, laborious, sensitive to errors, and has a small risk of adverse effects (Hall, 1971; Machleder et al., 1972). Clearly, an accurate non-invasive procedure for obtaining the arterial input function would be advantageous.

Alternative methods for characterising the (arterial) input function include the use of arterialised venous blood samples (Phelps et al., 1979) and population-based input functions (Takikawa et al., 1993). A widely used method for determining the input function in heart studies is to extract the input function from the PET images themselves (Gambhir et al., 1989; van der Weerdt et al., 2001). This idea was extended to brain studies by manually drawing regions of interest (ROIs) on larger arterial vessels, such as the carotid arteries, either directly on the PET images themselves (Chen et al., 1998; Wahl et al., 1999) or on co-registered high resolution magnetic resonance (MR) images (Litton, 1997). Alternative methods are the use of cluster analysis (Guo et al., 2003; Liptrot et al., 2004), independent component analysis (Naganawa et al., 2005a,b) or multiple linear regression analysis (Fang et al., 2004).

A challenge of using image-derived input functions (IDIFs) in the brain is the limited diameter of even the largest cerebral arteries. The diameter of the carotid arteries is smaller or comparable to the spatial resolution of most PET scanners, which means that PET images have to be corrected for partial volume and

* Corresponding author. Fax: +31 020 444 3090.
E-mail address: j.mourik@vumc.nl (J.E.M. Mourik).
Available online on ScienceDirect (www.sciencedirect.com).

1053-8119/$ - see front matter © 2007 Elsevier Inc. All rights reserved.
doi:10.1016/j.neuroimage.2007.10.022

spill-over effects to recover the true radioactivity concentrations. Several partial volume and spill-over correction methods have been developed based on determining the true cerebral blood vessel diameter using MRI (Rousset et al., 1998), (simple) mathematical functions (Sanabria-Bohorquez et al., 2003; Wahl et al., 1999), or least-square fitting to determine blood vessel and background geometries (Asselin et al., 2004).

The purpose of the present study was to validate a new method that combines correction for partial volume effects (spill-in and spill-out) during reconstruction with a simple procedure for extracting an IDIF from dynamic PET images. To this end, the reconstruction based partial volume correction method (Brix et al., 1997a; Reader et al., 2003) was used to improve spatial resolution and recover the true radioactivity concentration. Several ROI-based methods for defining the carotid arteries were evaluated. IDIFs and blood sampler input functions (BSIFs) were compared using areas under the curve (AUC) of input functions themselves and using final outcome of tracer kinetic analyses.

Materials and methods

Scan procedure

[^{11}C]flumazenil data of 10 subjects from ongoing clinical studies were included. All studies had been approved by the medical ethics committee of the VU University Medical Center and all subjects had given informed consent prior to scanning.

Scans were acquired using an ECAT EXACT HR+ scanner (CTI/Siemens, Knoxville, TN, USA). Before tracer administration, a 10-min transmission scan was acquired in 2D mode using 3 rotating ^{68}Ge/^{68}Ga sources. This scan was used to correct the subsequent emission scan for attenuation. Subsequently, a dynamic emission scan with a duration of 60 min was acquired in 3D acquisition mode, following bolus injection of 370±45 MBq (mean±S.D.) [^{11}C]flumazenil. This dynamic scan consisted of 16 time frames with variable frame lengths (4×15, 4×60, 2×150, 2×300 and 4×600 s) and during this scan the arterial input function was measured using a continuous flow-through automatic blood sampling device (Boellaard et al., 2001b). At set times (2.5, 5, 10, 20, 30, 40 and 60 min after injection), continuous withdrawal was interrupted briefly for the collection of manual samples and, after each sample, the arterial line was flushed with heparinised saline. These manual samples were used for calibrating the (on-line) blood sampler, for measuring plasma to whole blood ratios, and for determining plasma metabolite fractions.

Reconstruction based partial volume correction

The reconstruction based partial volume correction method of Brix et al. (1997a) and Reader et al. (2003) was used. This partial volume corrected ordered subsets expectation maximization (PVC-OSEM) reconstruction is based on the normalization and attenuation weighted (NAW) OSEM algorithm (Hudson and Larkin, 1994; Johnson et al., 1996; Shepp and Vardi, 1982). A schematic diagram of NAW-OSEM is given in Fig. 1.

The PVC-OSEM reconstruction algorithm improves the in-plane resolution of a PET image by taking into account the point-spread function (PSF) of the imaging system. To this end, the forward projection of the estimated image EI is blurred with a Gaussian-shaped distribution kernel representing the PSF of the system (smoothed image SI). As schematically illustrated in Fig. 2, in PVC-OSEM the updated sinogram US is calculated as the ratio between measured sinogram MS and *smoothed* estimated sinogram SES, finally resulting in a sharper representation of EI.

For computational speed, clinical use, and ease of implementation, a number of assumptions and/or approximations were used:

(1) It was assumed that the 3D point spread function (PSF) of the scanner is spatially invariant. This seems a reasonable assumption, as subjects were always placed in nearly the same position within the FOV. Therefore, the carotid arteries, used for IDIF, were at approximately the same position within the FOV (<2 cm) for all scans with little variation in local PSF between studies.
(2) Reconstruction was implemented using Fourier rebinning (FORE) (Defrise et al., 1997), followed by 2D NAW-OSEM or 2D PVC-OSEM, to allow for reconstruction of 3D dynamic scans within clinically feasible times (<15 h) on a SUN UltraSPARC-III workstation (440 MHz, 512 MB RAM).
(3) Use of the 3D PSF was included in the forward projection step only. Although in general it is assumed that the PSF should be included in both forward and back projections, preliminary studies indicated that this approach reduced convergence speed, resulting in the need for more iterations and thus very long reconstruction times (>24 h), without providing more accurate IDIFs.

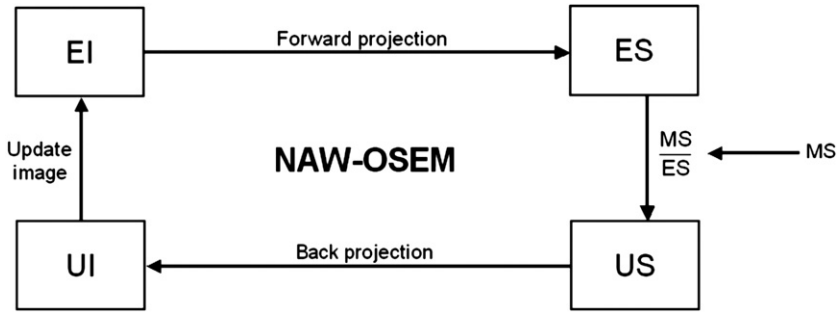

Fig. 1. Schematic representation of the normalization and attenuation weighted ordered subset expectation maximization (NAW-OSEM) reconstruction algorithm. An initial estimation of the PET image EI is forward projected to generate an estimated sinogram ES. The update sinogram (US=measured sinogram MS/ES) is calculated and back projected to create an update image UI. EI will then be updated according to $EI_{iter}=EI_{iter-1}$ *$UI_{iter}/(A+N)$, with A and N the attenuation and normalization weighting factors. The whole procedure is repeated for a set of iterations.

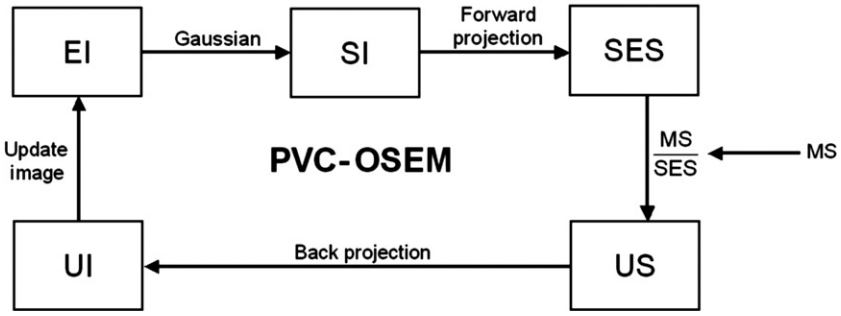

Fig. 2. Schematic representation of the partial volume OSEM (PVC-OSEM) reconstruction method. PVC-OSEM is a regular NAW-OSEM (Fig. 1) algorithm, except that during reconstruction it corrects for partial volume by taking the spatial resolution of the scanner into account.

Resolution measurement

The resolution of the ECAT EXACT HR+ scanner was measured using an ^{11}C point source. This point source was scanned at 0, 2.5 and 5 cm from the centre of the scanner (both transaxial and axial). Scans were reconstructed using filtered back projection (FBP) with a ramp filter at Nyquist frequency, as recommended by NEMA standards, and using an image matrix size of 1024 × 1024 voxels and a zoom factor of 2.0, resulting in images consisting of 63 planes with a voxel size of 0.32 × 0.32 × 2.43 mm^3. Next, the point spread function (PSF) and the mean FWHM (full width at half maximum) over all directions for all point source positions were determined.

Reconstruction settings

All data were normalised and corrected for attenuation, random coincidences, scattered radiation, dead time and decay and reconstructed using NAW-OSEM (2 iterations, 16 subsets) as implemented in the standard ECAT 7.2 software (CTI/Siemens, Knoxville, TN, USA) and afterwards smoothed with a Gaussian kernel of 5 mm resulting in an image resolution of 7 mm FWHM (standard setting for clinical studies). Additionally, PVC-OSEM images were reconstructed using various numbers of iterations and subsets (2 × 8, 2 × 16, 4 × 16, 6 × 16 and 8 × 16). The size of the Gaussian kernel representing the PSF of the tomograph was set at the outcome of the resolution measurement, as will be discussed later. All reconstructed images consisted of 63 planes of 256 × 256 voxels with a voxel size of 1.29 × 1.29 × 2.43 mm^3. PVC-OSEM images were only used for extracting IDIFs.

Region of interest definition

ROIs were defined on pseudo blood volume images, derived from the summation of early time frames ranging from 15 to 45 s post injection. These early time frames were chosen, because in this window the carotid arteries could easily be identified (Fig. 3). ROIs were defined on 11 successive planes, starting 3 planes below the circle of Willis. This volume (177.7 mm^3) corresponds to the position of the carotid arteries (Fig. 4) outside the skull to avoid spill-in from activity within the brain. The ROIs were defined (semi-) automatically on NAW-OSEM images and then projected onto PVC-OSEM images to extract whole blood time activity curves (TACs). Calibration of all reconstruction methods used (including PVC-OSEM) were verified prior to this study using phantoms.

Several methods for (semi-)automatic definition of ROIs were investigated:

A. *Automatic threshold*.
   - A1. Percentage of the maximum pixel value (60, 70, 80%) of the PET volume.
   - A2. Number of hottest pixels in *a volume* (10, 20, …, 60 pixels).
   - A3. Number of hottest pixels *per plane* (4, 6, …, 12 pixels).

B. *Semi-automatic simplified seeded region growing*. The simplified seeded region growing method (Adams and Bischof, 1994) only depends on a pixel threshold value and needs one starting seed for each carotid artery. For every pixel in a seed (initially one), the algorithm investigates whether

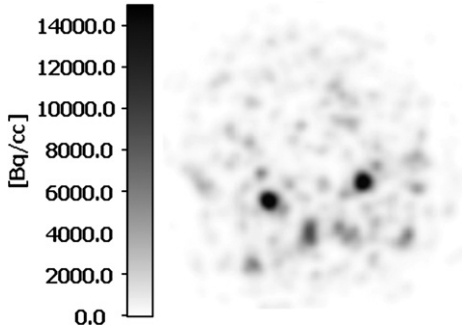

Fig. 3. Example of one plane of a pseudo blood volume image, consisting of a summed image of frames 2 and 3, 15–45 s after injection. The carotid arteries are clearly visible.

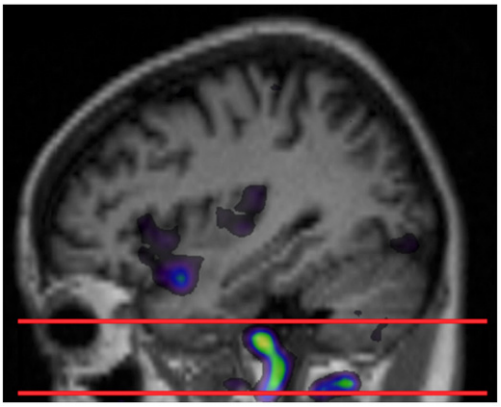

Fig. 4. Volume for defining ROIs over the carotid (between the two lines).

neighbouring pixels satisfy the threshold criteria. Neighbouring pixels that pass the threshold criteria will be added to the seed. The seeded region growing algorithm stops if no more pixels are added. In the present study both manual and automatic (50% of maximum pixel value of PET volume) thresholds were used.

C. *Cluster analysis*. Images were divided into 3, 4, 6, 8 and 10 clusters using the method described by Ashburner et al. (1994).

D. *Manually drawn ROI on magnetic resonance images (MRI)*. T1-weighted structural MRI scans were acquired using a 1.5 Tesla Sonata MRI system (Siemens, Erlangen, Germany). MRI scans were co-registered with summed NAW-OSEM scans (10–60 min) using a mutual information image registration algorithm (Maes et al., 1997). ROIs were manually drawn on the co-registered MRI images and copied to the PET scan.

Once the ROIs were defined they were copied to all frames of the PVC-OSEM dynamic scan. In addition, ROIs were also copied to all frames of the NAW-OSEM dynamic scan. The whole blood TACs were generated as the time sequence of the averaged ROI values. ROI definition and whole blood TAC extraction were all performed using dedicated in-house developed software within Matlab 7.1 (The Mathworks, Natick, MA, USA). The optimal settings for ROI definition were assessed based on AUC results of a preliminary study of four subjects.

Corrections and calibration

Blood sampler (BS) whole blood curves were calibrated based on the manual samples and corrected for delay. Image derived whole blood TACs were used both without and with calibration based on manual samples. Both BS whole blood curves and image derived whole blood TACs were corrected for plasma to whole blood ratios and metabolites. Metabolite correction was performed by multiplication of the plasma curves with a Hill-type function fit to the measured parent fraction, resulting in BS input functions (BSIFs) and image derived input functions (IDIFs). This Hill-type function is given by $M_p(t) = \frac{\alpha t^\beta}{t^\beta + \gamma}$, where $M_p(t)$ is the metabolite fraction in plasma as function of time t, and α, β and γ are fit parameters (Gunn et al., 1998; Lubberink et al., 2004b).

Tracer kinetic analysis

For both a BSIF and the various corresponding IDIFs, the AUC for peak (first 2 min) and tail (2–60 min) were calculated. In addition, peak to tail ratios were calculated for BSIF and IDIFs. Next, parametric volume of distribution (V_T) images were calculated for both BSIF and IDIFs using Logan analysis (Logan, 2000). In addition, V_T and K_1 images were calculated using a basis function method (BFM) (Boellaard et al., 2005; Gunn et al., 1997) of the single tissue compartment model. Logan and BFM parametric images were generated using the in-house developed software package PPET (Boellaard et al., 2006). Using the software package DISPLAY (Montreal Neurological Institute, http://www.bic.mni.mcgill.ca/software/Display/Display.html), a total of 15 ROIs were drawn manually on Logan V_T images in anatomical areas with varying levels of [^{11}C]flumazenil uptake (frontal, temporal and occipital cortex, white matter, thalamus, putamen, cerebellum, and pons). These manually defined ROIs were projected onto Logan V_T, and BFM V_T and K_1 images. Mean Logan V_T, and BFM V_T and K_1 for all anatomical regions were calculated for both BSIF and IDIFs. Mean parametric values (V_T or K_1) of BSIF were plotted against corresponding IDIF values. In addition, slope, intercept and Pearson's correlation coefficient (R^2) were calculated for each subject.

Results

Resolution measurement

Based on the ^{11}C point sources measurements a resolution of 4.3 mm FWHM at the centre of the scanner was found. The resolution decreased to 4.5 mm FWHM at 2.5 cm and to 4.8 mm FWHM at 5 cm from the centre, respectively.

Reconstruction settings

Fig. 5 shows the mean AUC over all subjects ($n=10$) of the first 2 min (peak) for both NAW-OSEM and PVC-OSEM reconstructions, the latter with different numbers of iterations. For PVC-OSEM a Gaussian kernel of 4.5 mm was used, based on the results of the resolution measurements. It can be seen that the AUC of the peak for standard (no PVC) NAW-OSEM is around 50% lower than that for BSIF. Good correspondence was found between AUC of BSIF and PVC-OSEM with 4, 6 or 8 iterations. AUC differences between the different iterations were small (<4%), but the S.D. increased with more than 30% when more than 4 iterations were used. Differences between AUCs of the tails were small compared to those of the peak. Based on these results and the fact that computational time increased with the number of iterations, all PVC-OSEM reconstructions were performed with 4 iterations and 16 subsets.

Region of interest definition

In the preliminary analysis of four subjects, use of the semi-automatic simplified seeded region growing ROI method (method B) resulted in low AUC ratios between BSIF and IDIF (peak: 0.70±0.15; tail: 0.83±0.15) for IDIF. Furthermore, whole blood TACs defined by cluster analysis (method C) were inaccurate and inconsistent with respect to the structures selected. Use of co-registered MRI images (method D) often resulted in erroneous

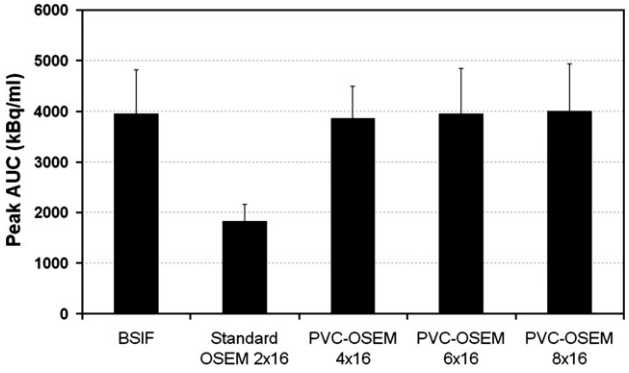

Fig. 5. Mean (±S.D.) AUC of the peak (first 2 min) for BSIF, IDIFs extracted from standard NAW-OSEM, and PVC-OSEM images. PVC-OSEM images are reconstructed using different numbers of iterations and subsets and a Gaussian kernel of 4.5 mm FWHM.

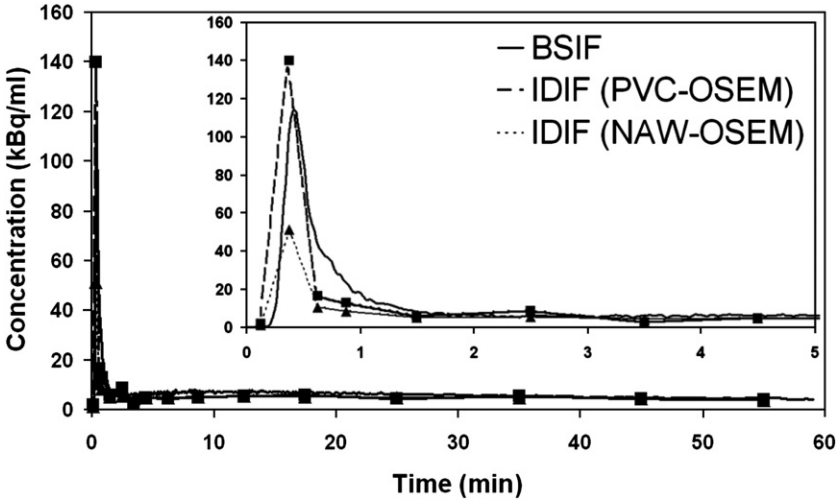

Fig. 6. Representative example of a whole blood BSIF and corresponding IDIFs extracted from PVC-OSEM and NAW-OSEM reconstructed images. Only BSIF was calibrated based on manual samples. The insert highlights the first 5 min.

definition of the carotid arteries, which in turn led to an underestimation of IDIF peak AUC values. Co-registration is based on the brain, but the carotid arteries are located outside the brain. Therefore, even an overall good co-registration can still lead to inaccurate co-registration of the carotid arteries, e.g. due to small image distortions (Sumanaweera et al., 1993) and/or differences in patient positioning between PET and MRI scans. Methods A1 (percentage of the maximum pixel value) and A2 (number of hottest pixels in a volume) were disregarded because they resulted in large variability amongst subjects, primarily due to the fact that often pixels outside the carotid arteries were included. This is explained by the large variability of the optimal threshold as function of object sizes comparable to the scanner resolution (van Dalen et al., 2007). Good correspondence between subjects and best AUC ratios (peak: 0.90±0.06; tail: 0.96±0.10) between BSIF and IDIF were achieved with method A3, i.e. the four hottest pixels per plane.

Calibration

A representative example of a BSIF and corresponding IDIFs, extracted from PVC-OSEM and NAW-OSEM reconstructed images, are shown in Fig. 6. For all subjects, the peak of the IDIF curve was reached slightly earlier and was sharper than that of the BSIF. BSIF and IDIFs were very well similar at later times. For PVC-OSEM reconstructed images, mean (±S.D.) AUC ratios ($n=10$) of IDIF without calibration and BSIF were 0.99±0.09 and 0.90±0.15 for peak and tail, respectively. For comparison, the same ratios for NAW-OSEM reconstructions were 0.47±0.06 and 0.81±0.08 for peak and tail, respectively.

Calibrating the IDIFs, extracted from PVC-OSEM reconstructed images, with manual samples resulted in AUC ratios between IDIF and BSIF of 1.13±0.28 and 1.00±0.06 for peak and tail, respectively.

Tracer kinetic analysis

Examples of parametric V_T and K_1 images obtained using BFM are shown in Fig. 7 for both BSIF and IDIF extracted from PVC-OSEM images. Correlations between BSIF and non-calibrated and calibrated IDIFs are shown in Figs. 8A and B respectively. Mean slope, intercept and R^2 of linear regression analyses between IDIF and BSIF for Logan derived V_T, and BFM derived V_T and K_1 over all subjects can be found in Figs. 9A–C, respectively. Significantly increased slopes for both Logan and BFM derived V_T (1.35±0.11 and 1.41±0.24, respectively) were found only for non-calibrated IDIFs from NAW-OSEM reconstructions (Figs. 9A, B). For all reconstructions investigated, nearly perfect intercept and R^2 values were found for Logan derived V_T (Fig. 9A). Variation was somewhat larger for BFM derived V_T, with some bias for NAW-OSEM derived IDIF (Fig. 9B). In case of both calibrated and non-calibrated IDIFs from NAW-OSEM reconstructions, high slopes

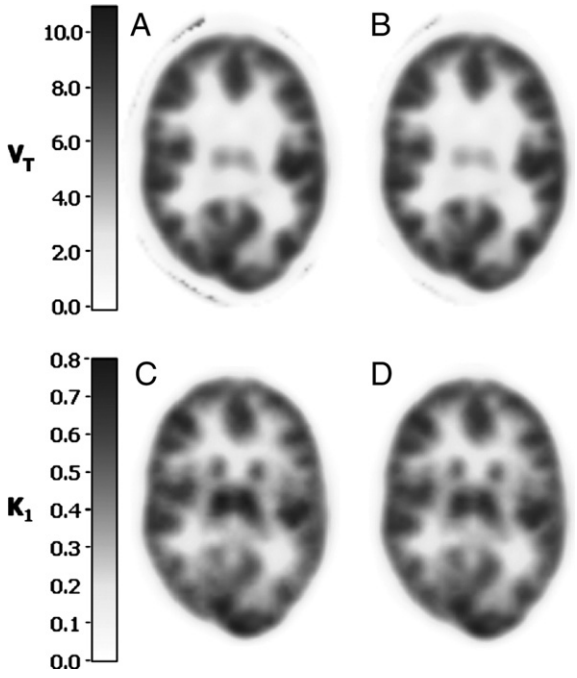

Fig. 7. Parametric V_T (A, B) and K_1 (C, D) images generated using BFM for BSIF (A, C) and non-calibrated IDIFs extracted from PVC-OSEM reconstructed images (B, D).

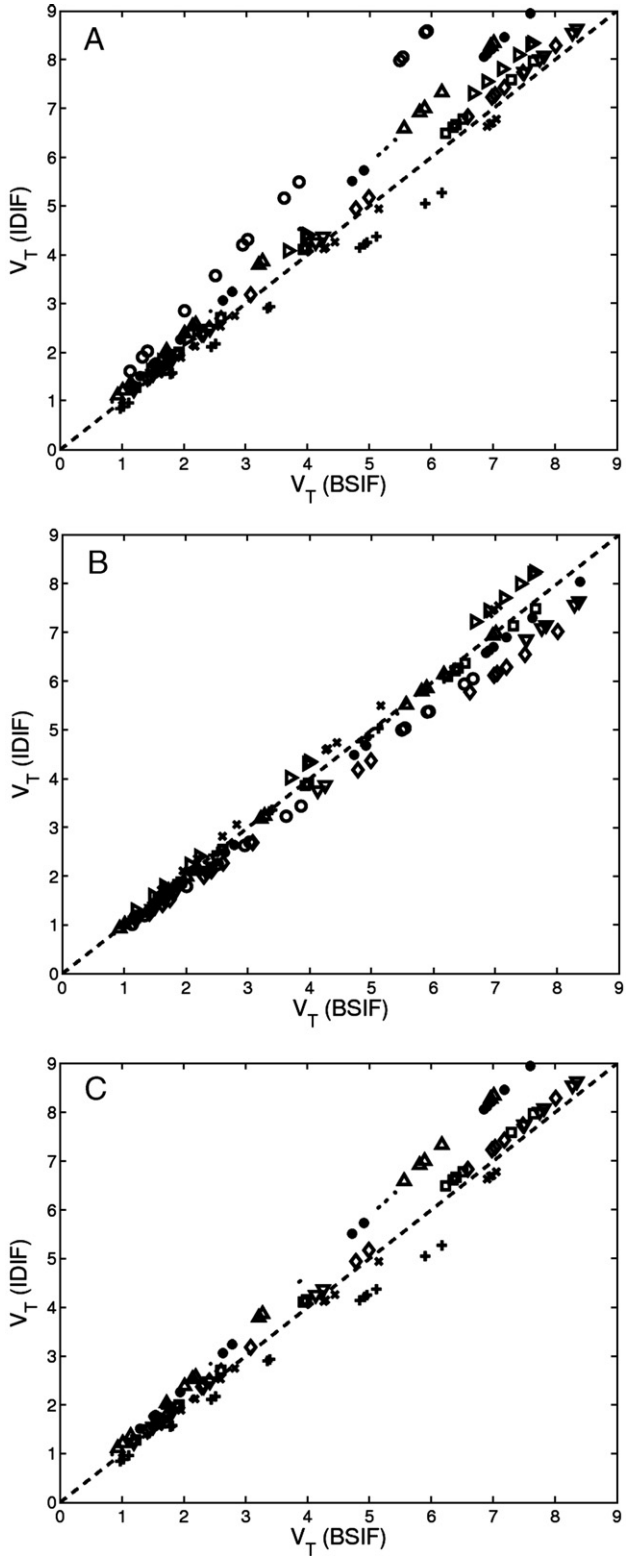

Fig. 8. Correlation between Logan derived V_T values using BSIF and (A) non-calibrated ($n=10$), (B) calibrated ($n=10$) and (C) non-calibrated IDIFs *without outliers* ($n=8$) extracted from PVC-OSEM images (-- line of identity). Every symbol represents a single subject (note that the same symbol per subject represents different anatomical regions).

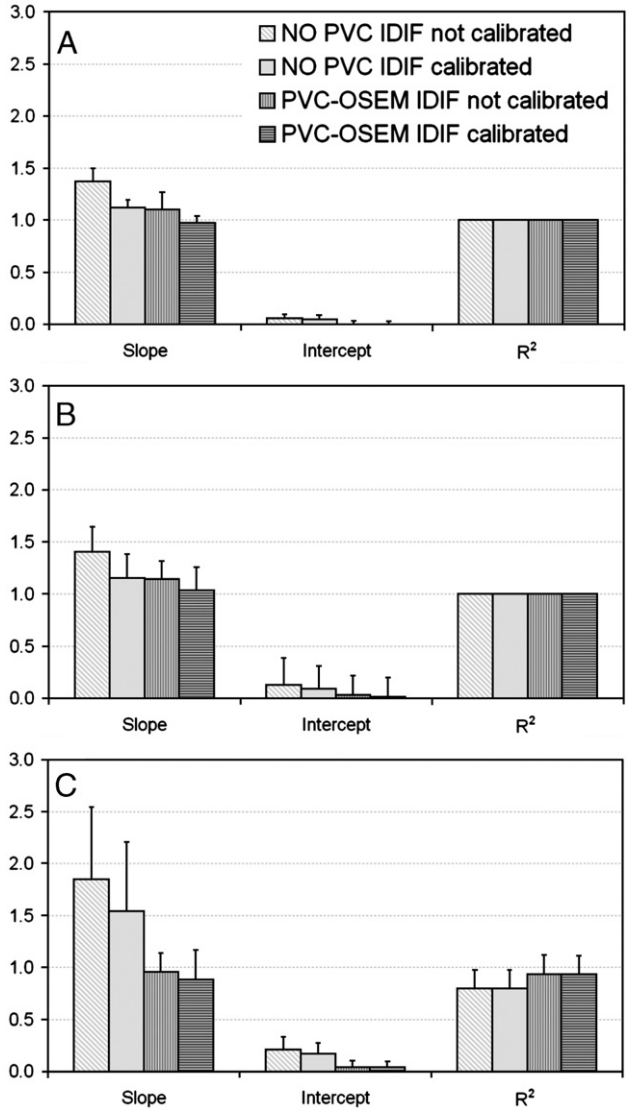

Fig. 9. Mean slope, intercept and R^2 for linear regression between IDIF and BSIF results for (A) Logan derived V_T, (B) BFM derived V_T, and (C) BFM derived K_1.

and intercepts, and low R^2 values, together with large standard deviations were found for BFM derived K_1 values (Fig. 9C). In general, much better results were obtained for IDIFs derived from PVC-OSEM reconstructions.

Discussion

PVC reconstruction settings

Previous studies have shown that the quantitative accuracy of OSEM reconstructions is comparable to the inherently quantitative filtered back projection (FBP) algorithm (Boellaard et al., 2001a; Lubberink et al., 2004a), also when using IDIFs. For the present study an OSEM reconstruction algorithm that corrects for partial volume effects was implemented. The optimal settings for the PVC-OSEM reconstruction algorithm combined a large recovery correction with a reasonable signal-to-noise ratio. As shown in Fig.

5 use of 4 iterations, 16 subsets and a PSF of 4.5 mm FWHM provided good correspondence between AUC (peak and tail) of blood sampler and image derived whole blood input, together with the low variance.

Results of the resolution measurements in the present study agree with the findings of Brix et al. (1997b). Using a steel needle ^{18}F line source, Brix et al. (1997b) measured the spatial resolution of the ECAT EXACT HR+ scanner and reported a FWHM of 4.4 mm at the centre of the field of view, degrading to approximately 4.8 mm at a distance of 5 cm from the scanner axis. In the present study a FWHM of 4.5 mm at a distance of 2.5 cm from the scanner axis was found, which on average is the position of the carotid arteries. It was therefore logical to use a resolution kernel of 4.5 mm for the PVC-OSEM algorithm. Although the true PSF of the ECAT EXACT HR+ scanner is not an exact Gaussian, it may be considered as a reasonable approximation of the PSF.

Region of interest definition

For the subgroup of four subjects included in preliminary study, using the four hottest pixels per plane gave the best AUC results for both peak and tail. AUC ratios between BSIF and IDIFs extracted from PVC-OSEM images even increased from 0.90±0.06 to 0.99±0.09 when all subjects were analysed. Compared with alternative ROI methods, use of the four hottest pixels is accurate, simple, largely automatic and fully reproducible. In addition, diameters of ROI defined with the four hottest pixels per plane did not overestimate the diameter of the carotid arteries (Krejza et al., 2006).

Calibration

In the calibration step, the *tail* of the IDIF was fitted to manual samples. In the present study the IDIF tail was on average lower than the samples. The AUC ratio for the tail between IDIF and BSIF increased from 0.90±0.15 to 1.00±0.06 after calibration of the IDIF. As a result, the AUC ratio for the peak also increased, overestimating the AUC of the peak by 13%. Note, however, that the latter value has a very large standard deviation. The overestimation may partly be explained by the contribution of two 'outlier' scans, as will be discussed later.

The differences between non-calibrated and calibrated IDIFs were rather small both for BFM and Logan derived V_T (Fig. 9). These small differences suggest that there is no real need to calibrate an IDIF with manual samples if V_T is the parameter of interest. Differences in slope values for BFM K_1 parametric images were much larger (calibrated: 0.88±0.28; non-calibrated: 0.96±0.17).

Although in many clinical studies where V_T is the parameter of interest manual samples are not needed for calibrating an IDIF, they are still required to correct the IDIF for plasma to whole blood ratios and for labelled metabolites. To further increase the clinical applicability of quantitative brain PET, future studies are needed to investigate the possibility of using a limited number (e.g. 7) of manual venous rather than arterial blood samples.

Tracer kinetic analysis

Differences between IDIFs extracted from NAW-OSEM and PVC-OSEM were large (Fig. 9). It is clear that results of PVC-OSEM are superior to those of NAW-OSEM. Therefore, in the remainder, only result of PVC-OSEM will be discussed.

As shown in Fig. 6, the peak of the IDIF was reached slightly earlier and was much sharper than that of the BSIF. This can be explained by the dispersion of the BSIF. Dispersion will lead to an underestimation of the peak height and a wider peak. The difference in top of the peak between BSIF and IDIF may be explained by small errors in the extrapolation algorithm.

In general, excellent correlations between IDIF and BSIF derived V_T and K_1 values were obtained. Especially correspondence of V_T values was excellent for PVC-OSEM reconstructions, although variability was slightly higher for BFM than for Logan analysis. On average, IDIF derived K_1 values were slightly lower than those obtained using BSIF. However, using a paired *t*-test, no significant differences in K_1 values between BSIF and non-calibrated IDIFs ($p=0.72$) as well as between BSIF and calibrated IDIFs ($p=0.45$) were found.

Outliers

The slope between BFM derived V_T values obtained with IDIF (not calibrated) and BSIF was relatively high for two subjects: 1.30 and 1.44, respectively. When these subjects were removed from the regression analysis, the mean slope decreased from 1.15±0.16 to 1.10±0.12 for BFM derived V_T (Fig. 10A) and from 1.10±0.17 to 1.06±0.12 for Logan derived V_T values (not shown). Both outliers also had a large effect on the R^2 values of BFM derived K_1 results, and especially on the variation of BFM derived K_1 values (Fig. 10B). AUC ratios between IDIF and BSIF for the tail increased from 0.90±0.15 (all subjects) to 0.94±0.13 (without outliers). No

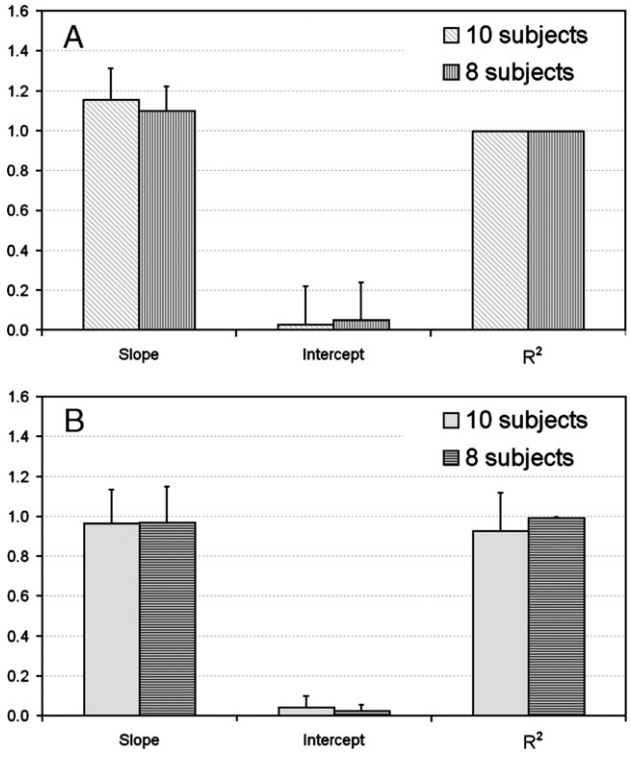

Fig. 10. Comparison of mean slope, intercept and R^2 for linear regression between non-calibrated IDIF and BSIF with and without inclusion of outliers for BFM derived (A) V_T and (B) K_1 values.

differences were found for peak AUC ratios. The sources of error for both outliers were carefully investigated.

One subject was considered to be an outlier based on the peak-to-tail ratio of the IDIF, which was outside the range of all other subjects ($p<0.05$), possibly due to motion artefacts. In case of the other subject, it was suspected that the BSIF was incorrect. This observation was confirmed when mean grey and white matter values for the K_1 images were calculated for all subjects. Two large ROIs were drawn in regions with mainly grey and white matter, respectively. Grey and white matter K_1 values were normal for IDIF, but compared to group average were significantly different for BSIF ($p<0.05$).

Comparison with other methods

Unlike other methods (Asselin et al., 2004; Chen et al., 1998; Naganawa et al., 2005a; Sanabria-Bohorquez et al., 2003; Su et al., 2005), the present method corrects for partial volume and spill-over effects by taking the scanner resolution into account *during* reconstruction. Sanabria-Bohorquez et al. (2003) used a mathematical function to correct for partial volume and spill-over effects, and also applied it to dynamic [^{11}C]flumazenil studies. They used manually drawn ROIs to define arteries and concluded that differences between BSIF and IDIF were mainly found during the first minutes after injection. After PVC, Sanabria-Bohorquez et al. (2003) found better V_T slopes (Sanabria-Bohorquez: [0.94…1.03]; present study without outliers: [0.85…1.19]), but poorer intercepts (Sanabria-Bohorquez: [−0.10…16]; present study without outliers: [−0.04…0.03]). Comparable R^2 values were found. For K_1 Sanabria-Bohorquez et al. (2003) found higher slope values, but in the present study much better R^2 values were found.

The proposed method for defining the blood pool is a simple, semi-automatic ROI method that is fully reproducible. Especially for clinical studies, this is a major advantage over other methods that use manually drawn ROIs (Sanabria-Bohorquez et al., 2003). Using the 'four hottest pixels per plane' is, however, dependent on voxel size, and therefore has to be evaluated for other settings than used in the present study. This is, however, also true for most other methods used to define blood vessels.

Limitations and clinical use

The main limitation of any IDIF method is its vulnerability to patient motion. In the present study, ROIs were defined on early time frames and then copied to all other frames. Patient motion at later times can easily lead to displacements of the carotid artery ROI in subsequent frames, leading to under- or overestimation of the true radioactivity. Although data were not conclusive, it is likely that patient motion played a role in at least one subject (one of the 2 outliers). To safeguard against patient movement a (frame-by-frame) motion correction algorithm (e.g. Andersson, 1995; Andersson, 1998; Woods et al., 1998a,b) could be implemented.

Arterial input as gold standard

According to common practice, the (externally measured) arterial input function was used as gold standard. Retrospective analysis, however, showed that the BSIF probably was not correct for at least one of the subjects. This conclusion was based on a comparison of the BSIF with those of the other subjects. It is by no means certain, however, that the other BSIFs are fully correct, as smaller deviations are more difficult to detect. In addition, in practice there are problems with cannulation or clogged lines in ~5% to 10% of cases, leading to study rejection. Clearly, use of a reliable IDIF would overcome at least some of these problems, especially when venous samples could substitute the arterial samples. Additionally, venous samples instead of arterial samples could increase patient friendliness of PET procedures and thereby facilitate clinical use of quantitative PET studies. One way of using venous samples is to transform measured venous blood samples into corresponding predicted arterial concentrations (Syvanen et al., 2006). Visvikis et al. (2004) showed that, for [^{18}F]FLT, there was no significant difference in determining metabolite fractions between venous and arterial samples. Clearly, these approaches need to be further substantiated for [^{11}C]flumazenil and other tracers. A very interesting alternative would be the approach of Sanabria-Bohorquez et al. (2000), who showed that, for [^{11}C] flumazenil, corrections for metabolites can be performed by including a mathematical solution during kinetic analysis.

Conclusion

In the present study, a method for extracting and improving accuracy of IDIFs from dynamic PET studies was developed. Accurate IDIFs were obtained using the four hottest pixels per plane, together with reconstruction based partial volume correction. AUC, Logan V_T, and BFM K_1 and V_T correlated well between IDIF and blood sampler derived data. No significant differences were found between calibrated and non-calibrated IDIFs, so manual samples were only necessary for calculating plasma to whole blood ratios and metabolites. Moreover, the observed IDIFs showed a higher and sharper peak in the input function, whilst the AUC of the peak was equal to that of the BSIF, suggesting that the difference in peak height might be due to dispersion of the BSIF. It appears that the proposed method is accurate, simple, fully reproducible and general enough to be applied to other tracers, although this needs to be validated in further studies. However, patient movement can be a limitation for use of IDIFs. Future studies need to focus on corrections for patient motion to improve accuracy of IDIFs. The present study, however, shows the feasibility of deriving accurate IDIFs from dynamic PET studies using reconstruction based PVC.

Acknowledgments

This work was financially supported by the Netherlands Organisation for Scientific Research (NWO, VIDI Grant 016.066.309). The authors would like to thank Floris H.P. van Velden and Dr. Bart N.M. van Berckel for their useful comments, Dr. Frederik Barkhof for the advice on MRI sequences and the PET radiochemistry and technology staff of the Division of Nuclear Medicine and PET Research for production of isotopes and acquisition of PET data.

References

Adams, R., Bischof, L., 1994. Seeded region growing. IEEE Trans. Pattern Anal. Mach. Intell. 16, 641–647.

Andersson, J.L., 1995. A rapid and accurate method to realign PET scans utilizing image edge information. J. Nucl. Med. 36, 657–669.

Andersson, J.L., 1998. How to obtain high-accuracy image registration:

application to movement correction of dynamic positron emission tomography data. Eur. J. Nucl. Med. 25, 575–586.

Ashburner, J., Haslam, J., Taylor, C., Cunningham, V.J., Jones, T., 1994. A cluster analysis approach for the characterization of dynamic PET data. In: Myers, R., Cunningham, V.J., Bailey, D., Jones, T. (Eds.), Quantification of Brain Function Using PET. Academic Press, San Diego, pp. 301–306.

Asselin, M.C., Cunningham, V.J., Amano, S., Gunn, R.N., Nahmias, C., 2004. Parametrically defined cerebral blood vessels as non-invasive blood input functions for brain PET studies. Phys. Med. Biol. 49, 1033–1054.

Boellaard, R., van Lingen, A., Lammertsma, A.A., 2001a. Experimental and clinical evaluation of iterative reconstruction (OSEM) in dynamic PET: quantitative characteristics and effects on kinetic modeling. J. Nucl. Med. 42 (5), 808–817 (May).

Boellaard, R., van Lingen, A., van Balen, S.C., Hoving, B.G., Lammertsma, A.A., 2001b. Characteristics of a new fully programmable blood sampling device for monitoring blood radioactivity during PET. Eur . J. Nucl. Med. 2001. 28 (1), 81–89 (Jan.).

Boellaard, R., Knaapen, P., Rijbroek, A., Luurtsema, G.J., Lammertsma, A.A., 2005. Evaluation of basis function and linear least squares methods for generating parametric blood flow images using 15O-water and Positron Emission Tomography. Mol. Imaging Biol. 7, 273–285.

Boellaard, R., Yaqub, M., Lubberink, M., Lammertsma, A.A., 2006. PPET: A software tool for kinetic and parametric analysis of dynamic PET studies. NeuroImage 31 (Supl. 2), T62.

Brix, G., Doll, J., Bellemann, M.E., Trojan, H., Haberkorn, U., Schmidlin, P., Ostertag, H., 1997a. Use of scanner characteristics in iterative image reconstruction for high-resolution positron emission tomography studies of small animals. Eur. J. Nucl. Med. 24, 779–786.

Brix, G., Zaers, J., Adam, L.E., Bellemann, M.E., Ostertag, H., Trojan, H., Haberkorn, U., Doll, J., Oberdorfer, F., Lorenz, W.J., 1997b. Performance evaluation of a whole-body PET scanner using the NEMA protocol National Electrical Manufacturers Association. J. Nucl. Med. 38, 1614–1623.

Chen, K., Bandy, D., Reiman, E., Huang, S.C., Lawson, M., Feng, D., Yun, L.S., Palant, A., 1998. Noninvasive quantification of the cerebral metabolic rate for glucose using positron emission tomography, 18F-fluoro-2-deoxyglucose, the Patlak method, and an image-derived input function. J. Cereb. Blood Flow Metab. 18, 716–723.

Defrise, M., Kinahan, P.E., Townsend, D.W., Michel, C., Sibomana, M., Newport, D.F., 1997. Exact and approximate rebinning algorithms for 3-D PET data. IEEE Trans. Med. Imag. 16, 145–158.

Fang, Y.H., Kao, T., Liu, R.S., Wu, L.C., 2004. Estimating the input function non-invasively for FDG-PET quantification with multiple linear regression analysis: simulation and verification with in vivo data. Eur. J. Nucl. Med. Mol. Imaging 31, 692–702.

Gambhir, S.S., Schwaiger, M., Huang, S.C., Krivokapich, J., Schelbert, H.R., Nienaber, C.A., Phelps, M.E., 1989. Simple noninvasive quantification method for measuring myocardial glucose utilization in humans employing positron emission tomography and fluorine-18 deoxyglucose. J. Nucl. Med. 30, 359–366.

Gunn, R.N., Lammertsma, A.A., Hume, S.P., Cunningham, V.J., 1997. Parametric imaging of ligand–receptor binding in PET using a simplified reference region model. NeuroImage 6, 279–287.

Gunn, R.N., Sargent, P.A., Bench, C.J., Rabiner, E.A., Osman, S., Pike, V.W., Hume, S.P., Grasby, P.M., Lammertsma, A.A., 1998. Tracer kinetic modeling of the 5-HT1A receptor ligand [carbonyl-11C]WAY-100635 for PET. NeuroImage 8, 426–440.

Guo, H., Renaut, R., Chen, K., Reiman, E., 2003. Clustering huge data sets for parametric PET imaging. Biosystems 71, 81–92.

Hall, R., 1971. Vascular injuries resulting from arterial puncture of catheterization. Br. J. Surg. 58, 513–516.

Hudson, H., Larkin, R., 1994. Accelerated image reconstruction using ordered subsets of projection data. IEEE Trans. Med. Imag. 13, 601–609.

Johnson, C., Seidel, J., Carson, R.E., Gandler, W.R., Sofer, A., Green, M.V., Daube-Witherspoon, M.E., 1996. Evaluation of 3D reconstruction algorithms for a small animal PET scanner. IEEE Trans. Nucl. Sci. 44, 1303–1308.

Krejza, J., Arkuszewski, M., Kasner, S.E., Weigele, J., Ustymowicz, A., Hurst, R.W., Cucchiara, B.L., Messe, S.R., 2006. Carotid artery diameter in men and women and the relation to body and neck size. Stroke 37, 1103–1105.

Lammertsma, A.A., Hume, S.P., 1996. Simplified reference tissue model for PET receptor studies. NeuroImage 4, 153–158.

Lammertsma, A.A., Bench, C.J., Hume, S.P., Osman, S., Gunn, K., Brooks, D.J., Frackowiak, R.S., 1996. Comparison of methods for analysis of clinical [11C]raclopride studies. J. Cereb. Blood Flow Metab. 16, 42–52.

Liptrot, M., Adams, K.H., Martiny, L., Pinborg, L.H., Lonsdale, M.N., Olsen, N.V., Holm, S., Svarer, C., Knudsen, G.M., 2004. Cluster analysis in kinetic modelling of the brain: a noninvasive alternative to arterial sampling. NeuroImage 21, 483–493.

Litton, J.E., 1997. Input function in PET brain studies using MR-defined arteries. J. Comput. Assist. Tomogr. 21, 907–909.

Logan, J., 2000. Graphical analysis of PET data applied to reversible and irreversible tracers. Nucl. Med. Biol. 27, 661–670.

Lubberink, M., Boellaard, R., van der Weerdt, A.P., Visser, F.C., Lammertsma, A.A., 2004a. Quantitative comparison of analytic and iterative reconstruction methods in 2- and 3-dimensional dynamic cardiac 18F-FDG PET. J. Nucl. Med. 45, 2008–2015.

Lubberink, M., Greuter, H.N.J.M., Boellaard, R., Luurtsema, G., Lammertsma, A.A., 2004b. Effect of plasma metabolite correction accuracy on kinetic analysis in positron emission tomography. NeuroImage 22.

Machleder, H.I., Sweeney, J.P., Barker, W.F., 1972. Pulseless arm after brachial–artery catheterisation. Lancet 1, 407–409.

Maes, F., Collignon, A., Vandermeulen, D., Marchal, G., Suetens, P., 1997. Multimodality image registration by maximization of mutual information. IEEE Trans. Med. Imag. 16, 187–198.

Naganawa, M., Kimura, Y., Ishii, K., Oda, K., Ishiwata, K., Matani, A., 2005a. Extraction of a plasma time–activity curve from dynamic brain PET images based on independent component analysis. IEEE Trans. Biomed. Eng. 52, 201–210.

Naganawa, M., Kimura, Y., Nariai, T., Ishii, K., Oda, K., Manabe, Y., Chihara, K., Ishiwata, K., 2005b. Omission of serial arterial blood sampling in neuroreceptor imaging with independent component analysis. NeuroImage 26, 885–890.

Phelps, M.E., Huang, S.C., Hoffman, E.J., Selin, C., Sokoloff, L., Kuhl, D.E., 1979. Tomographic measurement of local cerebral glucose metabolic rate in humans with (F-18)2-fluoro-2-deoxy-D-glucose: validation of method. Ann. Neurol. 6, 371–388.

Reader, A.J., Julyan, P.J., Williams, H., Hastings, D.L., Zweit, J., 2003. EM algorithm system modeling by image-space techniques for PET reconstruction. IEEE Trans. Nucl. Sci. 50, 1392–1397.

Rousset, O.G., Ma, Y., Evans, A.C., 1998. Correction for partial volume effects in PET: principle and validation. J. Nucl. Med. 39, 904–911.

Sanabria-Bohorquez, S.M., Labar, D., Leveque, P., Bol, A., De Volder, A.G., Michel, C., Veraart, C., 2000. [11C]flumazenil metabolite measurement in plasma is not necessary for accurate brain benzodiazepine receptor quantification. Eur. J. Nucl. Med. 27, 1674–1683.

Sanabria-Bohorquez, S.M., Maes, A., Dupont, P., Bormans, G., de Groot, T., Coimbra, A., Eng, W., Laethem, T., De Lepeleire, I., Gambale, J., Vega, J.M., Burns, H.D., 2003. Image-derived input function for [11C] flumazenil kinetic analysis in human brain. Mol. Imaging Biol. 5, 72–78.

Shepp, L.A., Vardi, Y., 1982. Maximum likelihood reconstruction for emission tomography. IEEE Trans. Med. Imag. 1, 113–122.

Su, K.H., Wu, L.C., Liu, R.S., Wang, S.J., Chen, J.C., 2005. Quantification method in [18F]fluorodeoxyglucose brain positron emission tomography using independent component analysis. Nucl. Med. Commun. 26, 995–1004.

Sumanaweera, T.S., Glover, G.H., Binford, T.O., Adler, J.R., 1993. MR susceptibility misregistration correction. IEEE Trans. Med. Imag. 12, 251–259.

Syvanen, S., Blomquist, G., Appel, L., Hammarlund-Udenaes, M., Langstrom, B., Bergstrom, M., 2006. Predicting brain concentrations of drug using positron emission tomography and venous input: modeling of arterial–venous concentration differences. Eur. J. Clin. Pharmacol. 62, 839–848.

Takikawa, S., Dhawan, V., Spetsieris, P., Robeson, W., Chaly, T., Dahl, R., Margouleff, D., Eidelberg, D., 1993. Noninvasive quantitative fluorodeoxyglucose PET studies with an estimated input function derived from a population-based arterial blood curve. Radiology 188, 131–136.

van Dalen, J.A., Hoffmann, A.L., Dicken, V., Vogel, W.V., Wiering, B., Ruers, T.J., Karssemeijer, N., Oyen, W.J., 2007. A novel iterative method for lesion delineation and volumetric quantification with FDG PET. Nucl. Med. Commun. 28, 485–493.

van der Weerdt, A.P., Klein, L.J., Boellaard, R., Visser, C.A., Visser, F.C., Lammertsma, A.A., 2001. Image-derived input functions for determination of MRGlu in cardiac (18)F-FDG PET scans. J. Nucl. Med. 42, 1622–1629.

Visvikis, D., Francis, D., Mulligan, R., Costa, D.C., Croasdale, I., Luthra, S.K., Taylor, I., Ell, P.J., 2004. Comparison of methodologies for the in vivo assessment of 18FLT utilisation in colorectal cancer. Eur. J. Nucl. Med. Mol. Imaging 31, 169–178.

Wahl, L.M., Asselin, M.C., Nahmias, C., 1999. Regions of interest in the venous sinuses as input functions for quantitative PET. J. Nucl. Med. 40, 1666–1675.

Woods, R.P., Grafton, S.T., Holmes, C.J., Cherry, S.R., Mazziotta, J.C., 1998a. Automated image registration: I General methods and intrasubject, intramodality validation. J. Comput. Assist. Tomogr. 22, 139–152.

Woods, R.P., Grafton, S.T., Watson, J.D., Sicotte, N.L., Mazziotta, J.C., 1998b. Automated image registration: II. Intersubject validation of linear and nonlinear models. J. Comput. Assist. Tomogr. 22, 153–165.